JOURNAL OF MATERIALS SCIENCE **36** (2001) 2615–2619

Microstructure and properties of ceramic coatings produced on 2024 aluminum alloy by microarc oxidation

WENBIN XUE*, ZHIWEI DENG, RUYI CHEN, TONGHE ZHANG, HUI MA
Key Laboratory for Radiation Beam Technology and Materials Modification, Institute of Low Energy Nuclear Physics, Beijing Normal University, 100875 Beijing, People's Republic of China
E-mail: xuewb@263.net

The microstructures of the microarc oxidation coatings and 2024 aluminum alloy substrate were observed using the scanning electron microscope (SEM) and the phase composition of the coatings was analyzed by X-ray diffraction (XRD). Furthermore, the profiles of the nanohardness, *H*, and elastic modulus, *E*, along the coating depth were first determined using the mechanical properties microprobe. The microarc oxidation coatings consist of two layers—a loose layer and a compact layer. The *H* and *E* in the compact layer are about 18–32 GPa, 280–390 GPa, respectively. The *H* and *E* profiles are similar, and both of them exhibit a maximum value at a same depth of the coatings. The distribution of α-Al_2O_3 phase content determines the *H* and *E* profiles in the coatings. The changes of α-Al_2O_3 and γ-Al_2O_3 contents result from the different cooling rates of the molten alumina in the microarc discharge channel at the different depths of the coatings. After the microarc oxidation treatment, the microstructure of the alloy substrate, even near the Al/Al_2O_3 interface, has not been changed.

1. Introduction

Microarc oxidation is a new surface technology of producing ceramic coatings on valve metals, which is developed from anodic oxidation. In 1970s, Wirtz and his coworkers [1] successfully produced the ceramic coatings on Al alloys by utilizing DC spark discharge between electrodes in aqueous solution. This method was named anodic spark deposition (ASD) [2, 3]. Nevertheless, in Russia and China, similar ceramic coatings with better performance were obtained on the aluminum alloys using AC power supply and higher voltages comparing to ASD. However, this method was eventually named microarc oxidation (MAO) or microplasma oxidation [4–8].

In the process of MAO, Al substrate is directly oxidized to become α-Al_2O_3 and γ-Al_2O_3 phases due to a high temperature sintering in the microarc zone. So there is an ideal adhesion between the MAO coating and the metal substrate. The surface properties of the Al alloys, such as wear resistance, corrosion resistance, high temperature shock, electrical insulation, etc., can be surprisingly improved [9–11]. Applications are expected in many fields.

In this work, microstructure of the MAO coatings on 2024 aluminum alloy was observed using scanning electron microscope (SEM) with energy dispersive spectrometry (EDS). The nanohardness and elastic modulus profiles of the coatings were first determined using the mechanical properties microprobe. In addition, microarc oxidation mechanism was discussed.

2. Experimental procedure

In the experiment, ceramic coating was accomplished with a home-made 30 kW AC microarc oxidation system [6–8]. The service consists of a potential adjustable AC power supply up to 1000 V, a stainless steel container used as an electrolyte cell, and a stirring system and cooling system. The sample and container wall were used as two electrodes, respectively. Disks of Al-4.3Cu-1.5Mg 2024 alloy with a diameter of 40 mm × 7 mm were used as the primary samples. The electrolytic solution was the NaOH and additives. The current density was about 10 A/dm^2. The solution temperature was controlled to be under 35 °C. After mircoarc oxidation, the disks were cut and the metallographic specimens were prepared. Microstructure and composition in a cross-sectional specimen were analyzed using a Cambridge S-250 scanning electron microscope with EDS.

Nanoindention is a new method to determine the mechanical properties in a small area of materials. Nanohardness and elastic modulus measurements of the MAO coating and substrate were performed

* Author to whom all correspondence should be addressed.

using the mechanical properties microprobe (Nano Indenter II manufactured by Nano Instruments, Inc.) with load and displacement resolutions of 75 nN and 0.04 nm, respectively. A Berkovich indenter, a three-sided diamond pyramid with an area-to-depth function which is the same as that of a Vickers indenter, a four-sided diamond pyramid, was used in this work. The materials are characterized continuously by recording the relationship between the imposed load on the Berkovich indenter and the indenter displacement (namely penetration depth) during the indentation process. The total displacement contains the plastic component and elastic recovery during unloading, and the unloading curve was used to determine the elastic modulus and nanohardness of the specimen [12].

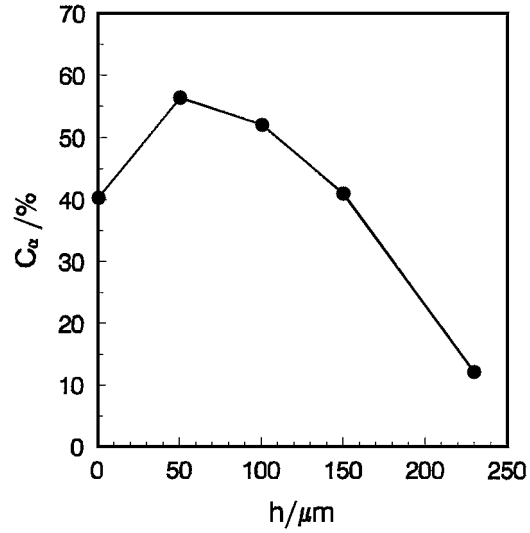

Figure 2 The distribution of α-Al_2O_3 content C_α along the depth of the coating formed on 2024 Al alloy by microarc oxidation.

3. Experimental results

3.1. Microstructure and phase composition of the MAO coatings

As shown in Fig. 1a, the alumina ceramic coating consists of a surface loose layer and a compact layer. The coating/substrate interface is clear, and no big voids can be observed near the interface. Furthermore, the thermal effect zone in the Al substrate near the interface can not be found.

Fig. 1b is a SEM backscattered electron image with Al line scanning near the coating/substrate. The contrast at two sides of the interface is rather high. The dark part is alumina coating, and the bright is Al substrate. No obvious transition layer can be observed. Some white particles appear in the substrate near the Al/Al_2O_3 interface, which are confirmed to be $CuMgAl_6$ phase using EDS analysis. It is specially worthy of attention that the morphology and distribution of these white particles at the interface are the same as those inside the alloy away from the interface. This confirms that the process of the instantaneous high temperature and high pressure in microarc discharge channel has no obvious effect on the microstructure of the alloy substrate. The microstructure of the substrate has not been changed, and the Al alloy substrate has not been remelted. Thus the temperature in the aluminum substrate must always be lower than the aluminum melting point of 660 °C during microarc oxidation.

In reference 6, we have determined the phase content distribution from the outer surface to the interior of the MAO coating on 2024 aluminum alloy using X-ray diffraction (XRD). However, the phase composition of the coating near the coating/substrate interface has not been determined. In present work, a similar sample was immersed in nitric acid solution to make the coating stripped from the alloy substrate. Then phase composition in the internal surface of the stripped coating was supplementarily determined by XRD. The MAO coating on 2024 Al alloy is mainly composed of α-Al_2O_3 and γ-Al_2O_3 phases. Supposing C_α and C_γ represent relative contents of the α-Al_2O_3 and γ-Al_2O_3 phases ($C_\alpha + C_\gamma = 1$), Fig. 2 [6] depicts the distribution of α-Al_2O_3 content C_α along the coating depth. The point for the internal surface of the coating in Fig. 2 ($h = 0\,\mu$m) was added according to the former XRD analysis. By comparing Fig. 1 and Fig. 2, the loose layer consists of about 88 wt% of α-Al_2O_3 and of about 12 wt% of γ-Al_2O_3. The contents in the compact layer are approximate 50 wt% respectively. From the surface layer to the interior of the MAO coating, the C_α gradually increases while the C_γ reduces. However, C_α at the 50 μm depth from the Al/Al_2O_3 interface amounts to a maximum value, then it decreases near the interface.

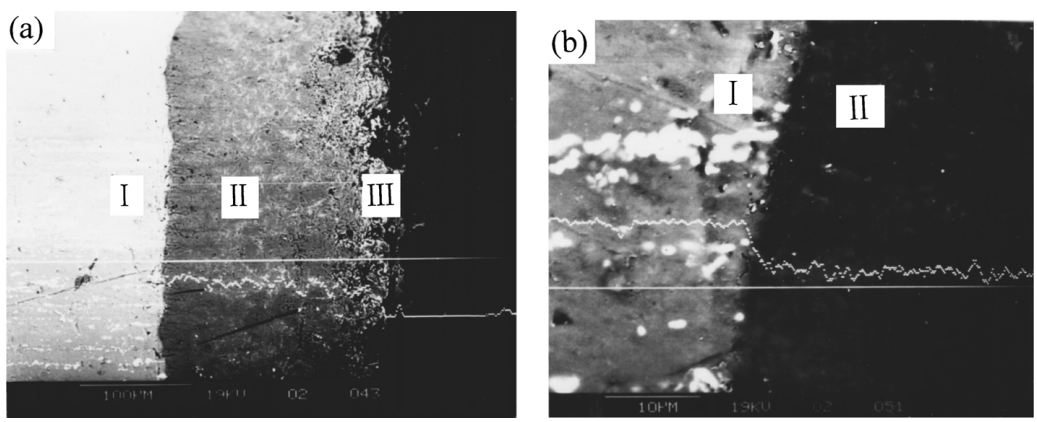

Figure 1 SEM micrographs of a cross-section sample with the coating formed by microarc oxidation on 2024 Al alloy, I the alloy substrate, II the compact layer, III the loose layer. (b) is a magnified image of (a) near the interface.

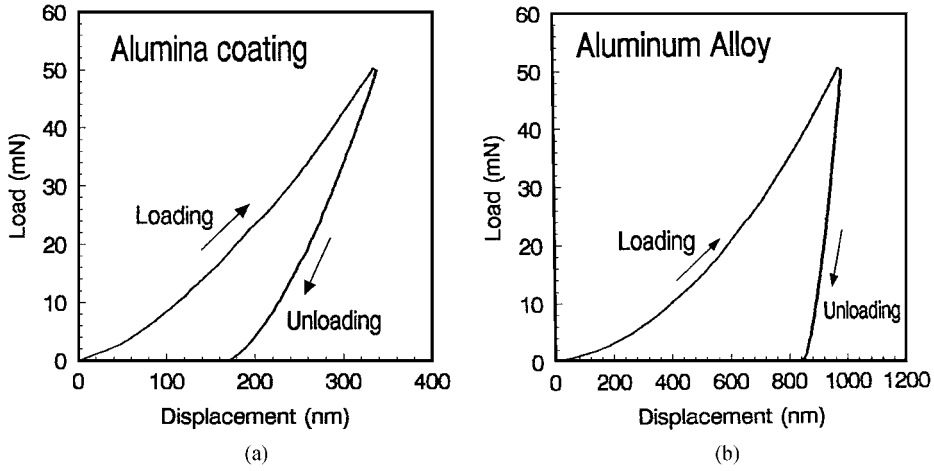

Figure 3 Typical load-displacement curves for an alumina coating and Al alloy. (a) alumina coating, (b) Al alloy substrate.

3.2. Nanoindentation test

3.2.1. Load-displacement curves for alumina coating and Al alloy

Typical load-displacement curves for the alumina coating and substrate, obtained using the mechanical properties microprobe, are shown in Fig. 3. The loading and unloading curves are not linear. Under the peak load of 50 mN (5.1 g), the maximum displacement (penetration depth) for the Al alloy is much larger than for the alumina coating. It is seen that a great deal of the peak-load displacement in Fig. 3a is elastically recovered on unloading and reaches 50% of the maximum displacement, which is the characteristic of an alumina ceramic [12]. On the contrary, elastic recovery for the Al alloy substrate in Fig. 4b is only 15%, and the peak-load displacement derives mostly from plastic deformation.

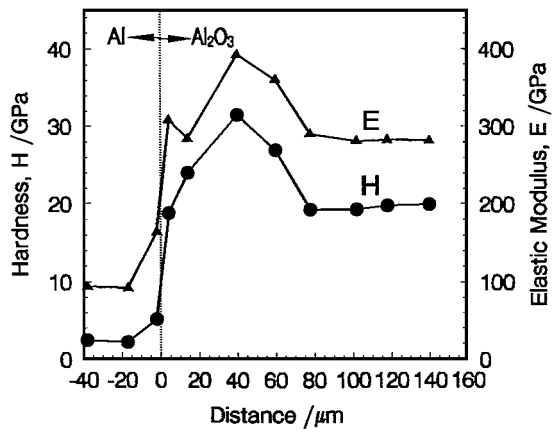

Figure 4 Profiles of nanohardness, H, and elastic modulus, E, for the MAO coating and 2024 Al alloy substrate under the 50 mN load.

3.2.2. Distributions of nanohardness and elastic modulus

Fig. 4 illustrates the distributions of nanohardness (H) and elastic modulus (E) of the MAO ceramic coating on 2024 aluminum alloy under the 50 mN load. The nanohardness profile in Fig. 4 is similar to the microhardness profile determined by Vickers microhardness tester [5–8]. H and E in the compact layer are in the range of 18–32 GPa and 280–90 GPa, respectively. The curve profiles of H and E distributions are very similar. From the Al/Al_2O_3 interface to the outer layer of the coating, H and E first increase gradually with distance, then both of them reach maximum values at same distance of 40 μm from the interface. After crossing the maximum values, they begin to decrease with distance. In the region of 80–140 μm, H and E approximately remain no change. Surprisingly, elastic modulus of the coating at the 14 μm distance away from the interface is slightly lower than at the 4 μm distance. It might result from the heterogeneous distributions of the α-Al_2O_3 and γ-Al_2O_3 phases in the local area of the coating, and further research should be done. Some researchers [5] suggested that a transition layer of several micrometers exists in the coating adjacent to the interface, where the microhardness is as low as the substrate. But in present paper, nanoindentation experiment with a very small load shows the hardness of the coating is rather high even near the interface, and no such layer with a lower hardness could be identified (see Fig. 4). Furthermore, microstructure near the interface also shows that no transition layer of an Al and Al_2O_3 mixture appears (see Fig. 1).

Nanohardness, H, and elastic modulus, E, of the coating near the Al/Al_2O_3 interface are still rather high. For example, H and E of the alumina coating, 4 μm away from the interface, reach 18 GPa and 300 GPa, respectively. It seems that they are not much influenced by the Al substrate because both the diameter and depth of the indentation in peak load are only about 2 μm and 0.4 μm, respectively. Due to a very high hardness of the MAO coating, a larger load has to be used for conventional Vickers microhardness test so that the indentation is large enough to measure [5–8]. In this case, for the MAO coating near the interface, the measured Vickers microhardness would be much lower than the actual value, because the influence of the Al substrate on the microhardness of the coating near the interface will be rather large. However, the mechanical properties microprobe can accurately determine H and E of the MAO coating near the Al/Al_2O_3 interface under a very small load. That indicates the advantage of nanoindentation method on determining H and E of the microarc oxidation coating.

3.2.3. Analysis of nanoindentation at the interface

Fig. 5 depicts indentations in the Al substrate near the Al/Al_2O_3 interface. The bright region around the indentation can be seen, which is caused by the pile-up effect [13, 14], namely, the volume of aluminum material displaced by the indentation pushes out to the sides of the indenter. One angle of the indentation centred at 2 μm away from the interface has pressed into the coating adjacent to the interface. Hence, H and E of 5.147 GPa and 164 GPa respectively, derived from load-displacement data in this indenting point, are composite values of Al alloy and alumina (see Fig. 4). As a matter of fact, actual nanohardness and elastic modulus at this position are lower than the measured values, and they should not be much higher than in the substrate far from the interface.

Due to the particularity of this indentation point adjacent to interface shown in Fig. 5, the load-displacement curve is plotted in Fig. 6. By compared with Fig. 3, it is seen that unloading curve in Fig. 6 is different from that in Fig. 3. There is a point of inflection B in unloading curve AC, and the slope of line BC is much smaller than that of line AB and similar to that in alumina. It is believed that in the AB part of unloading curve in Fig. 6, the Berkovich indenter still keeps contact with both alumina coating and the Al alloy substrate. Of course, most of the contact area is related to the substrate. While the unloading reaches the point of inflection B, the indenter begins to leave the substrate but continues to keep contact with the coating adjacent to the interface, as the elastic recovery of the coating with high elastic modulus is much larger than that of Al alloy. Hence, the line AB of unloading curve reflects the composite properties of Al and Al_2O_3 in agreement with the result shown above. However the line BC only reflects Al_2O_3 properties. It should be noted that the E and H in nanoindentation experiment are related to the slope of unloading curve during initial stage of unload but are independent of the line BC in Fig. 6.

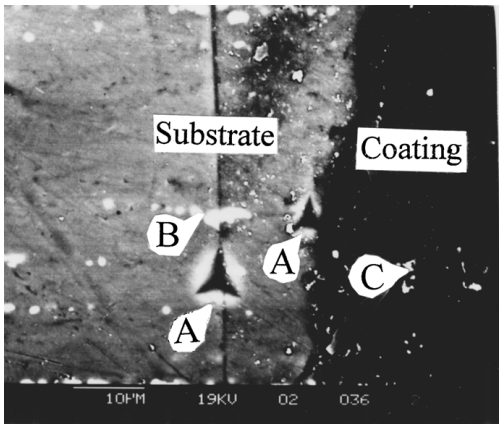

Figure 5 A SEM micrograph of 50 mN indentations in the Al substrate near the interface. A, pile-up effect area around the indentation. B, $CuMgAl_6$ phase. C, contaminated particle during mechanical polishing of the sample.

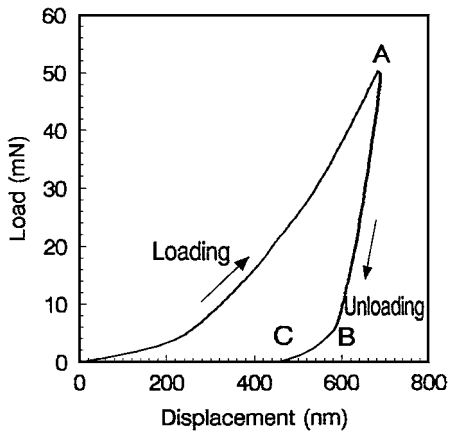

Figure 6 Load-displacement curve for the indentation in the Al alloy substrate adjacent to the interface with 2 μm.

4. Discussion

Microarc oxidation employs a higher voltage, which is different from anodic oxidation. At the initial stage of microarc oxidation, a thin insulating film of anodic oxidation is quickly formed on the surface of Al alloy in a suitable electrolyte solution. While the voltage between the anode and cathode goes up and is over a critical value, the film is locally broken and spark or microarc discharges appear. If this higher voltage is held, many bright sparks cover the whole surface of the Al alloy, and the spark or microarc spots move on the surface rapidly. Although the life of each spark is very short, the plasma atmosphere is formed in those small discharge zones where the instantaneous temperature can be over 7000 K [15]. So the oxide coating may be locally and temporarily molten. During microarc oxidation, the sample is always kept on room temperature due to aqueous solution cooling; meanwhile, the local high temperature is also made in microarc discharge channels. This is an important feature of microarc oxidation differing from anodic oxidation.

It is usually believed that the amorphous MAO alumina coating is first produced. The amorphous phase is first transformed into γ-Al_2O_3, and then γ-Al_2O_3 phase is yet transformed into α-Al_2O_3 by heating in the range of 800–1200 °C. We have proposed a new formation mechanism of the MAO coatings to explain the distributions of α-Al_2O_3 and γ-Al_2O_3 phase contents from the surface layer to the interior of the coatings [6]. The main idea of this mechanism is that both α-Al_2O_3 and γ-Al_2O_3 phases in the MAO coatings are mainly formed through rapid solidification of the molten alumina. The critical free energy of nucleation for γ-Al_2O_3 is lower than for α-Al_2O_3 while there is a very high cooling rate. So the γ-Al_2O_3 content in the outer layer of the coatings, contacted with aqueous solution, is higher due to a high cooling rate. Furthermore, from the surface to the interior of the coating, the γ-Al_2O_3 content gradually decreases and the α-Al_2O_3 content correspondingly increases. This is in good agreement with the XRD analyses as shown in Fig. 2.

However, this mechanism is also available for the whole oxide coatings. In the process of microarc oxidation, each microplasma discharge channel like one tube has extented to the Al/Al_2O_3 interface from the coating surface. The molten alumina in microarc discharge

zone has a very high cooling rate at the surface layer of the coatings contacted with the solution. However, its cooling rate at the part contacted with the alloy substrate is also much higher than the interior of the coatings. Hence, γ-Al_2O_3 content in the coating near the Al/Al_2O_3 interface should be also rather high. In a certain scope of the coating depth, α-Al_2O_3 content C_α increases with increasing the distance from the interface, on the contrary, γ-Al_2O_3 content C_γ gradually decreases ($C_\gamma = 1 - C_\alpha$). Since the cooling rate of the molten alumina varies with the coating depth, there is an extreme value in the profiles of both α-Al_2O_3 and γ-Al_2O_3 contents versus the coating depth. The distribution of α-Al_2O_3 content C_α at the different depth of the coatings determines the H and E profiles in the MAO coatings. Therefore, the H, E, C_α profiles in the MAO coatings are similar, and have an intrinsic relation. This is in good agreement with the experiments above.

The diameter in a microarc discharge channel is only several microns or less, and the lifetime of each spark or microarc is less than one millisecond. Furthermore, the solidification rate of the molten alumina near the Al/Al_2O_3 interface is very high. So the process of the instantaneous high temperature and pressure in the microarc discharge zone would have no obvious influence on the substrate microstructure. Hence, the microstructure and mechanical properties of the Al alloy substrate remains the same as mentioned above.

5. Conclusions

(1) The ceramic coatings formed on 2024 aluminum alloy by microarc oxidation consist of two layers, a loose layer and a compact layer. The nanohardness, H, and elastic modulus, E, in the compact layer are 18–32 GPa, 280–390 GPa, respectively. The H and E profiles in the coatings are similar. Each of them has a maximum value at the same depth of the coatings.

(2) The distribution of the α-Al_2O_3 phase content in the coatings has also a maximum value, and it determines the H and E distributions. The changes of α-Al_2O_3 and γ-Al_2O_3 contents result from the difference of cooling rate of the molten alumina in the microarc discharge channels at the different depth of the coatings.

(3) Although the local melt of oxide coating has taken place due to the microarc sintering, the Al substrate near the interface has not been remelted and its microstructure has not been changed.

Acknowledgments

This research was sponsored by the national "863" high-tech program of China (715-011-020), the national natural science foundation of China (59801003) and Beijing new-star program for science and technology (9558102500). The authors wish to thank Miss Danmei Liu and Miss Qing Zhao, of state key laboratory for Advanced Metals and Materials in University of Science and Technology Beijing for assisting in the nanoindentation experiments.

References

1. T. B. VAN, S. D. BROWN and G. P. WIRTZ, *Am. Ceram. Soc. Bull.* **56**(6) (1977) 563.
2. G. P. WIRTZ, S. D. BROWN and W. M. KRIVEN, *Mater. Manu. Processes* **6**(1) (1991) 87.
3. J. P. SCHRECKENBACH, G. MARX, F. SCHLOTTIG, M. TEXTOR and N. D. SPENCER, *J. Mater. Sci.: Mater. in Medicine* **10** (1999) 453.
4. A. V. TIMOSHENKO and YU. V. MAGUROVA, *Zashch. Met.* **31**(5) (1995) 523 (in Russian).
5. V. MALYSCHEV, *Metalloberfläche* **49**(8) (1995) 606.
6. WENBIN XUE, ZHIWEI DENG, YONGCHUN LAI and RUYI CHEN, *J. Amer. Ceram. Soc.* **81**(5) (1998) 1365.
7. WENBIN XUE, ZHIWEI DENG, RUYI CHEN and TONGHE ZHANG, *Thin Solid Films* **372** (2000) 114.
8. WENBIN XUE, YONGCHUN LAI, ZHIWEI DENG and RUYI CHEN, *Mater. Sci. Technol.* **7**(2) (1999) 18 (in Chinese).
9. A. I. SLONOVA, O. P. TERLEYEVA, E. K. SHULEPKO and G. A. MARKOV, *Elektrochimiya* **28**(9) (1992) 1280 (in Russ.)
10. A. L. YEROKHIN, A. A. VOEVODIN, V. V. LYUBIMOV, J. ZABINSKI and M. DONLEY, *Surf. Coat. Technol.* **110** (1998) 140.
11. X. NIX, A. LEYLAND, H. W. SONG, A. L. YEROKHIN, S. J. DOWEY and A. MATTHEWS, *ibid.* **116–119** (1999) 1055.
12. W. C. OLIVER and G. M. PHARR, *J. Mater. Res.* **7**(6) (1992) 1564.
13. A. BOLSHAKOV and G. M. PHARR, *ibid.* **13**(4) (1998) 1049.
14. K. W. MCELHANEY, J. J. VLASSAK and W. D. NIX, *ibid.* **13**(5) (1998) 1300.
15. M. D. KLAPKIV, *Mater. Sci.* **31**(4) (1995) 494.

Received 17 August
and accepted 27 November 2000